Journal of Macromolecular Science, Part A
Publication details, including instructions for authors and subscription information:
http://www.informaworld.com/smpp/title~content=t713597274

Equilibrium Sorption of Hexavalent Chromium from Aqueous Solution Using Iron(III)-Loaded Chitosan-Magnetite Nanocomposites As Novel Sorbent

S. K. Bajpai[a]; Mukesh Kumar Armo[b]
[a] Polymer Research Laboratory, Department of Chemistry, Govt. Model Science College, Jabalpur, M. P., India [b] Department of Chemistry, Govt. Chandra Vijay College, Dindori, M. P., India

To cite this Article Bajpai, S. K. and Armo, Mukesh Kumar(2009) 'Equilibrium Sorption of Hexavalent Chromium from Aqueous Solution Using Iron(III)-Loaded Chitosan-Magnetite Nanocomposites As Novel Sorbent', Journal of Macromolecular Science, Part A, 46: 5, 510 — 520
To link to this Article: DOI: 10.1080/10601320902797764
URL: http://dx.doi.org/10.1080/10601320902797764

Journal of Macromolecular Science®, Part A: Pure and Applied Chemistry (2009) **46**, 510–520

ISSN: 1060-1325 print / 1520-5738 online
DOI: 10.1080/10601320902797764

Taylor & Francis
Taylor & Francis Group

Equilibrium Sorption of Hexavalent Chromium from Aqueous Solution Using Iron(III)-Loaded Chitosan-Magnetite Nanocomposites As Novel Sorbent

S. K. BAJPAI[1,*] and MUKESH KUMAR ARMO[2]

[1]*Polymer Research Laboratory, Department of Chemistry, Govt. Model Science College, Jabalpur (M. P.) 482001, India*
[2]*Department of Chemistry, Govt. Chandra Vijay College, Dindori (M. P.) 481880, India*

Received October 2008, Accepted November 2008

This work describes magnetic separation of hexavalent chromium by iron(III)-loaded chitosan-magnetite nanocomposites. The Cr(VI) uptake data, studied at 25°C and 45°C, was well fitted into the Freundlich isotherm. The values of constant K_F and 1/n were found to be 1.515, 1.266 and 1.006 (mg g^{-1}) (l $mg^{-1})^{1/n}$ and 0.76, 0.77, and 0.71, respectively. The Dubinin-Kaganer-Radushkevich isotherm was applied to determine mean sorption energy E. The value of E was found to be in the 8.977 to 9.90 kJ mol^{-1} range, thus indicating the chemical nature of the sorption process. The kinetics of Cr(VI) uptake was best interpreted by the Power function model. The intraparticle diffusion of sorbate was confirmed by the Bangham equation, and various thermodynamic parameters were also evaluated. Finally, a plausible mechanism has been suggested to understand the sorption process. The intraparticle diffusion was found to occur and later on confirmed by the Bangham equation. Finally, a plausible mechanism has been suggested for the observed Cr(VI) uptake on this newly developed sorbent. The various thermodynamic parameters were also evaluated.

Keywords: Sorption, chitosan, magnetite, Freundlich, power law

1 Introduction

Hexavalent chromium, one of the potential pollutants with a well known toxicity (1), is used extensively in industries such as electroplating, tanning, anodizing and chrome mining. Strong exposure of Cr(VI) may cause cancer in the digestive tract and lungs (2). Although, the mechanistic cytotoxity of Cr(VI) is not completely understood, a number of studies have demonstrated that it induces oxidative stress, DNA damage and apoptotic cell death (3). Therefore, its removal from drinking water sources and industrial effluents has been a matter of great concern for environmental chemists. Most industries like paint and pigment manufacturing, leather tanning, chrome plating etc. in underdeveloped countries like India, discharge waste water into the surface water only after reduction of Cr(VI) into Cr(III). However, the major drawback of this conventional treatment method is the high cost of chemicals used for reduction purpose and incomplete reduction of Cr(VI) which may produce toxic sludge due to surface adsorption of Cr(VI) onto a Cr(III) hydroxide precipitate. Therefore, it is essential to develop cost-effective technologies that can minimize the Cr(VI) concentration to the 'below toxic level' without producing any adverse effects on the environment. In the recent past, there have been remarkable attempts made for removal of hexavalent chromium from aqueous solutions using cost-effective and non-toxic naturally occurring sorbent materials such as chitosan (4), saw dust (5), wood-pulp (6), oil palm fibers (7), coconut coir (8) brown coals (9), sodium alginate (10), cajanus cajan husk (11), lignocellulosic residues (12) etc. However, due to practical problems associated with these sorbent materials, such as their tendency to agglomerate, their sticky nature and problems in packing the columns or in removal of these sorbents after the sorption process is over, these materials have been confined to laboratory experiments only and their uses on industrial scale have not been as attractive.

Magnetic separation appears to be the best alternative to overcome such problems. Due to the magnetic nature of the sorbent material, its removal from the sorption system can easily be done by introducing a moderate magnetic field onto the sorption system. In addition, the nanoscale size of sorbent enhances its surface area appreciably, thus

*Address correspondence to: S. K. Bajpai, Polymer Research Laboratory, Department of Chemistry, Govt. Model Science College, Jabalpur (M. P.) 482001, India. E-mail: mnlbpi@rediffmail.com; sunil.mnlbpi@gmail.com

causing effective removal of toxic metals (13). Recently, Bajpai et al (14) have demonstrated effective removal of Cr(VI) by using magnetite nanoparticles. In addition, maghemite nanoparticles have also been used for removal of Cr(VI) from aqueous solutions (15). The maximum adsorption was observed at pH 2.5 and the uptake data was well fitted in the Freundlich model. Magnetic alginate microcapsules have also been exploited for the removal of Ni(II) from aqueous solutions (16).

Most recently, Shehaand and co-worker (17) have successfully removed Cr(VI) using a new organic-inorganic magnetic composite resin, obtained by immobilizing magnetite within the polymer poly(acrylic acid-acrylonitrile) and the ion exchange resin (Amberlite IR 120). In this continuation, we hereby propose a unique 'already used magnetic sorbent' for the effective magnetic separation of another toxin chromium(VI). In our previous work, we reported chitosan-magnetite nanocomposites for the removal of iron(III) (18). Here, we propose the effective removal of hexavalent chromium by re-using the iron(III)-loaded chitosan-magnetite nano-composite (ILCMN) as a new magnetic sorbent material. To the best of our knowledge, such a sorbent-sorbate system has been reported for the first time.

2 Experimental

2.1 Materials

Chitosan was obtained by de-acetalylation of chitin (Hi Media, Mumbai, India) under strong alkaline conditions as reported previously (19). Its molecular weight, as determined using the Mark-Howink equation, was found to be 6.1×10^5. The chemicals ferrous chloride, ferric chloride, sodium hydroxide, potassium dichromate were purchased from Hi Media Laboratories, Mumbai, India and were used as received. The double distilled water was used throughout the investigations.

2.2 Preparation of Magnetite Nanoparticles

Magnetite nanoparticles were prepared by chemical co-precipitation of Fe(II) and Fe(III) ions in a strong alkaline solution of sodium hydroxide followed by treatment under hydrothermal conditions. Iron(II) and iron(III) chloride were dissolved in 1:2 molar ratios in distilled water and chemically precipitated at 40°C by adding 30% NaOH dropwise with constant stirring, at a control pH (10–10.4). The suspension was heated at 90°C for one hour under continuous stirring and separated by centrifuging several times in water and then in ethanol at 200 rpm. The purification step was used to remove impurities from Fe_3O_4nanoparticles. The particles were finally dried in vacuum at 70°C. The jet-black appearance of freshly prepared Fe_3O_4 nanoparticles and their retention by magnet were indications of magnetite formation.

2.3 Preparation of Chitosan-Magnetite Nanocomposites (CMN)

The pre-calculated quantity of magnetite nanoparticles was added to a 1%(w/v) solution of chitosan obtained by dissolving chitosan in 2% (v/v) acetic acid solution. The above colloidal suspension was stirred at a constant rate and was allowed to be dropped into a 2M sodium hydroxide solution under constant stirring. The magnetite-chitosan nanocomposites, thus obtained were filtered and washed extensively with water until neutrality was almost obtained. Finally the solid mass was dried at 50°C in an electric oven.

2.4 Preparation of Iron(III)-loaded CMN (ILCMN)

The known quantity of CMN was added to an aqueous solution (w/v) of $FeCl_3$ and the resulting mixture was stirred vigorously at a constant rate for a period of 2 h. The obtained iron(III)-loaded CMN was filtered, washed with distilled water, and then dried in an electric oven (Tempstar, India) at 40°C. The iron(III) uptake by CMN was determined by measuring the equilibrium concentration (i.e., C_e) of iron(III) solution using a spectrophotometric method (20). The solid dried mass was passed through standard sieves to get micrometer sized ILCMN particles of average geometrical diameters, 84 μm and 508 μm. We shall designate them as ILCMN (84) and ILCMN (508), respectively. Figure 1 (A) and (B) depicts the physical appearance of magnetite and iron(III)-loaded CMN, respectively.

2.5 FTIR Spectroscopy

The FTIR spectra of magnetite, plain chitosan and chitosan-magnetite nanocomposites was recorded by FTIR spectrophotometer, (Shimadzu, 8201) using KBr.

2.6 TEM Analysis

The TEM image was obtained by employing a JEM-2010 microscope under 200 kV. The samples for observation of TEM were prepared by placing a few drops of magnetite and CMN suspensions prepared in acetone, on the carbon-coated copper grid and allowing them to dry.

2.7 TGA analysis

Thermal analysis of chitosan and chitosan magnetite nanoparticles was carried out using a thermogravimetric analyzer (Metler, Toledo Gmb H Switzerland). About 9.6 mg of a powdered sample was placed in ceramic crucibles and analyzed over the temperature range of 20 to 600°C at

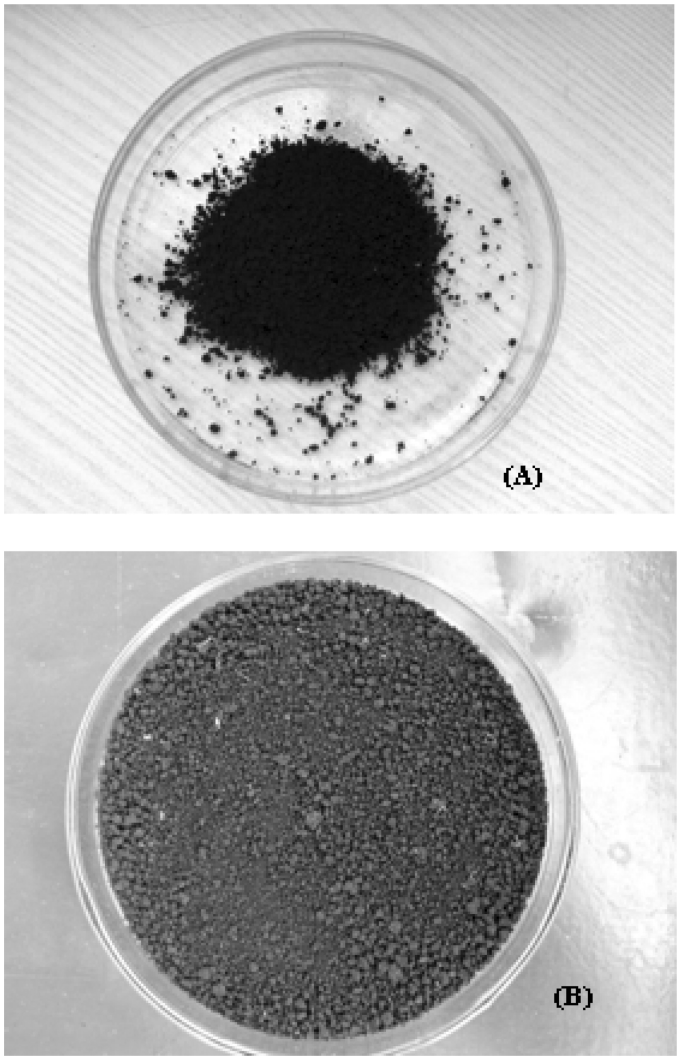

Fig. 1. Photograph of (A) magnetite and (B) chitosan-magnetite nanocomposite (CMN).

a heating rate of 20°C per min under the flow of dry N_2 at the rate of 30 ml min^{-1}.

2.8 Cr (VI) Uptake Studies

The stock solution of $K_2Cr_2O_7$ was prepared by dissolving its pre-calculated quantity in distilled water to give a final concentration of 50 mg l^{-1}. The stock solution was diluted to obtain standard solutions with their concentration in the range of 1 to 10 mg l^{-1}. Now, 50 ml of $K_2Cr_2O_7$ solution of desired concentration was placed in a 125 ml Erlenmeyer flask containing 20 mg of sorbent ILCMN and agitated in thermostatic water bath at 50 rpm for 2 h. At the end of the experiment, the sorbent particles were removed from the sorption system by introducing a bar magnet and supernatant was analyzed for a Cr(VI) concentration using the diphenylcarbazide method (21).

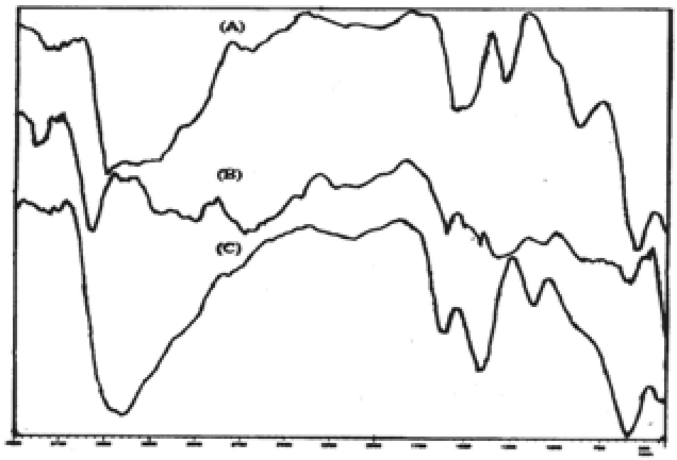

Fig. 2. FTIR spectrum of magnetite, plain chitosan and iron (III)-loaded chitosan-magnetite nanocomposite.

3 Results and Discussion

3.1 FTIR Spectral Analysis

The formation of chitosan-magnetite nanocomposites (CMN) was confirmed by FTIR spectral analysis (Figure 2). In (A), a characteristic peak of magnetite, present at 610 cm^{-1} confirms the metal-oxygen stretching, whereas in (B) the peaks corresponding to stretching vibrational frequency of amide I and amide II of chitosan molecules appeared at 1650 and 1449 cm^{-1}. Finally, it can be seen in (C) that all these characteristic peaks are present in the spectrum at chitosan-magnetite nanocomposites.

3.2 TGA Analysis

Since thermal stability of magnetite is more than that of the polymer chitosan, its doping into the chitosan is expected to enhance the overall thermal stability of the resulting nanocomposite. The results of thermogravimetric analysis, as depicted in Figure 3, clearly indicate that the initial decomposition temperatures of plain chitosan and chitosan-magnetite nanocomposite (CMN) are 162 and 195°C, respectively. The higher decomposition temperature of CMN is due to the presence of magnetite in the nanocomposite material. In addition, the overall thermal decomposition of chitosan and CMN is observed to be nearly 69 and 27%, thus indicating enhanced thermal stability of CMN. Finally, the plain chitosan suffers a major weight loss of nearly 40% at 256°C, while at the same temperature; CMN shows a weight loss of nearly 8%. Thus, it may be concluded that CMN particles possess greater thermal stability than plain chitosan.

3.3 TEM Analysis of Magnetite Particles

Figure 4 shows a TEM image and Selected Area Electron diffraction (SAED) pattern of the synthesized magnetite

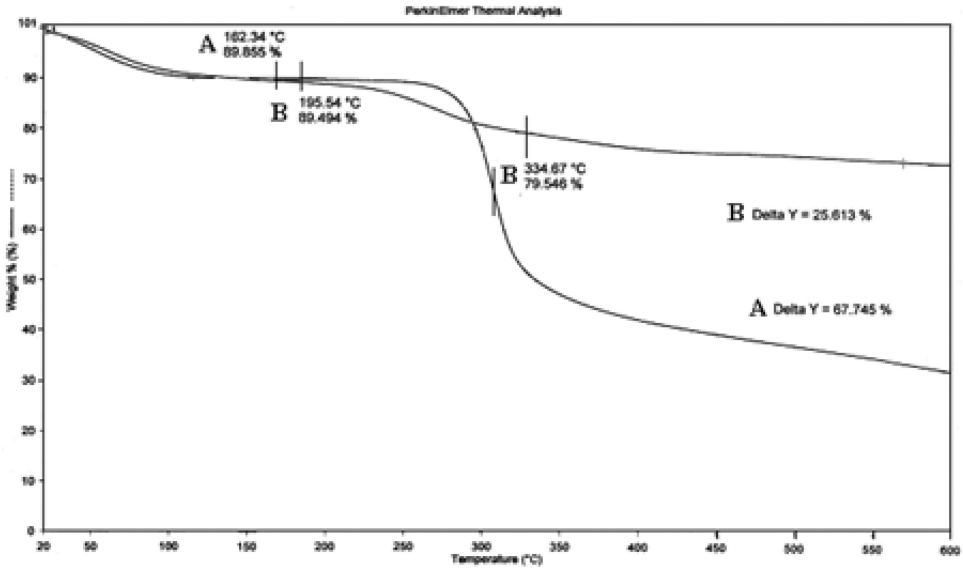

Fig. 3. Thermograms of plain chitosan and chitosan-magnetite nanocomposites.

nanoparticles. It is clear that most of the particles are almost monodisperse with an average of nearly 100 nm. The particles also seem to be aggregated which may be attributed to the absence of a stabilizer in the reaction system during the course of formation of magnetite. The SAED pattern also confirms formation of magnetite nanoperticles.

3.4 TEM Analysis of CMN Particles

The transmission electron microscopy (TEM) image of CMN particles has been shown in Figure 5. The average diameter of particles, as determined from the measurement of diameter of 15 particles selected from the TEM image in an arbitrary manner, was found to be nearly 29 nm. It also clear that the two moieties, namely chitosan and magnetite are homogeneously mixed or embedded into each other which may simply be attributed to the two simultaneous processes that occurred during the mixing of chitosan-magnetite suspension into an aqueous solution of sodium hydroxide. The exact mechanism of the formation of CMN has been well explained in our previous work (18).

3.5 Sorption Isotherms

The equilibrium sorption data can be regarded as an indication of attainment of equilibrium for the distribution of solute between the sorbent and sorbate phase and is usually interpreted in the terms of one or more isotherms (22). In the present study, the equilibrium Cr(VI) uptake data

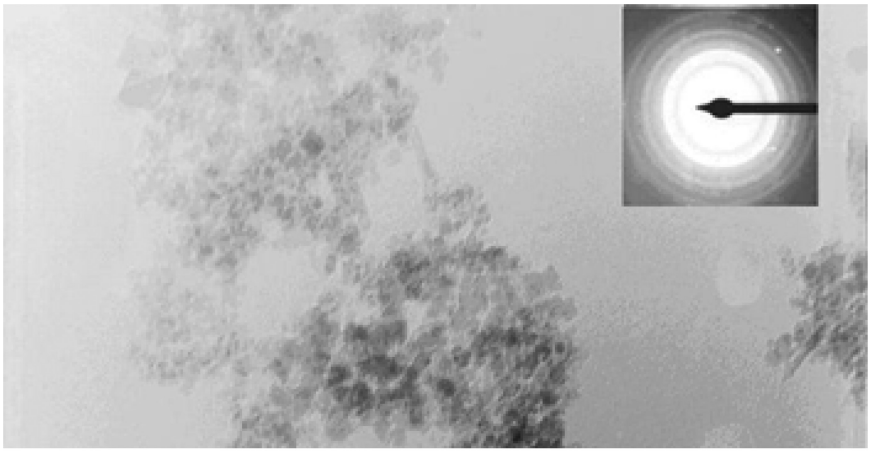

Fig. 4. TEM image of magnetite nanoparticles.

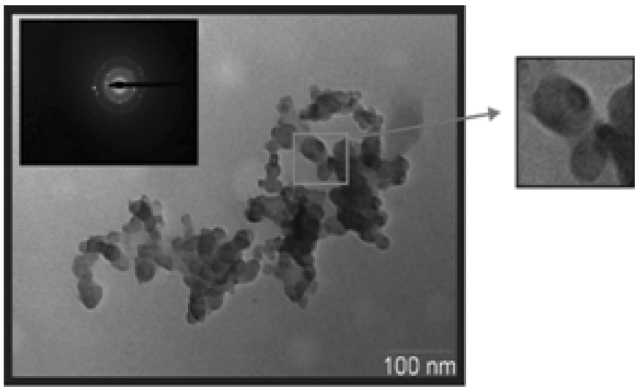

Fig. 5. TEM image of chitosan-magnetite nanocomposite (CMN).

was obtained by agitating 84 μm sized ILCMN particles in chromium (VI) solutions of different concentrations, in the range of 1 to 10 mg l^{-1}, at three different temperatures, namely 25, 35 and 45°C. The data, thus obtained, was fitted in the linearized Freundlich sorption isotherm:

$$\log q_e = \log K_F + 1/n \log C_e$$

Where Ce is the equilibrium concentration (mg l^{-1}) of Cr(VI) in the solution, q_e in the amount of sorbate present on sorbent at equilibrium (mg l^{-1}) and K_F and 1/n are Freundlich constants related to the maximum sorption capacity (mg g^{-1}) (l mg^{-1})$^{1/n}$ and energy of sorption (l mg^{-1}), respectively. The almost linear plots, obtained between log q_e and log C_e at three temperatures, with regression values in the range 0.9869 to 0.9907, indicated suitability of the Freundlich isotherm on the uptake data (Figure 6). The values of K_F and 1/n, as obtained using intercept and slope of the linear plots, have been given along with those obtained using regression analysis, in the Table 1. It can clearly be seen that the two values are in close agreement with each other. In addition, we also applied equilibrium sorption data on the Langmuir model (Figure 7). However, the poor regressions (0.782, 0.8553, 0.9164) obtained were indicative of unsuitability of the model. The Freundlich type of behavior is an indication of the surface heterogeneity of the sorbent i.e., the surface of the sorbent is made up of small heterogeneous adsorption patches that are homogeneous in themselves (23). In addition, as the values of 1/n lie in the range 1 to 10, the sorption capacity is quite fair (24).

Table 1. Graphical and regression values of Freundlich constant obtained for Cr(VI) uptake by 84 μm sized sorbent particles at different temperatures

	Graphical values			*Regression values*	
Temp. (°C)	K_F *(mg* g^{-1}*)* *(l* mg^{-1}*)*$^{1/n}$	*1/n*	R^2	K_F *(mg* g^{-1}*)* *(l* mg^{-}*)*$^{1/n}$	*1/n*
25	1.515	0.7683	0.9886	1.386	0.8590
35	1.266	0.7726	0.9907	1.169	0.8496
45	1.006	0.7116	0.9869	0.953	0.7600

In order to determine the nature of the sorption process, the equilibrium Cr(VI)-uptake data was applied on an DKR isotherm model (25) which, in the linearized form, may be given as:

$$\ln q_e = \ln X_m - \beta\varepsilon^2$$

Where q_e is the amount of Cr(VI) sorbed at equilibrium (mg g^{-1}), X_m is the DKR monolayer capacity, β is the activity coefficient related to the mean sorption energy and ε is the Polanyi potential, given as:

$$\varepsilon = RT \ln(1 + 1/Ce)$$

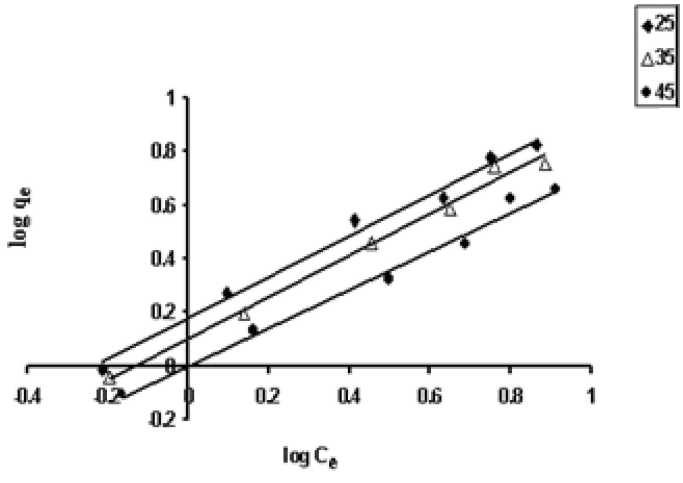

Fig. 6. Freundlich isotherm for Cr(VI) uptake at three different temperatures.

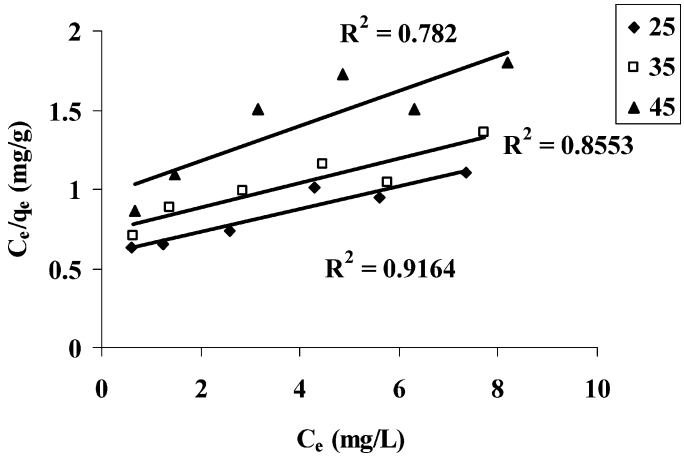

Fig. 7. Langmuir isotherm for Cr(VI) uptake at three different temperatures.

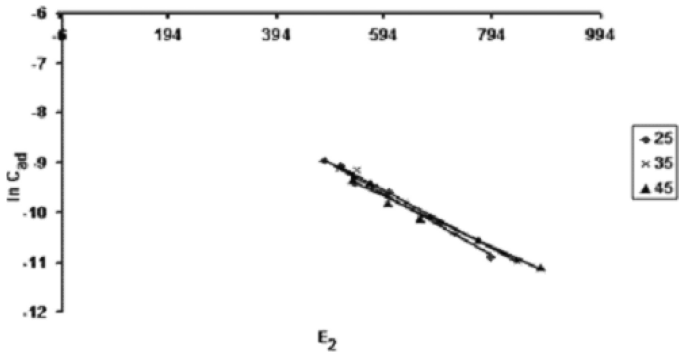

Fig. 8. Dubinin-Radushkevich isotherm of Cr(VI) for evaluation of β.

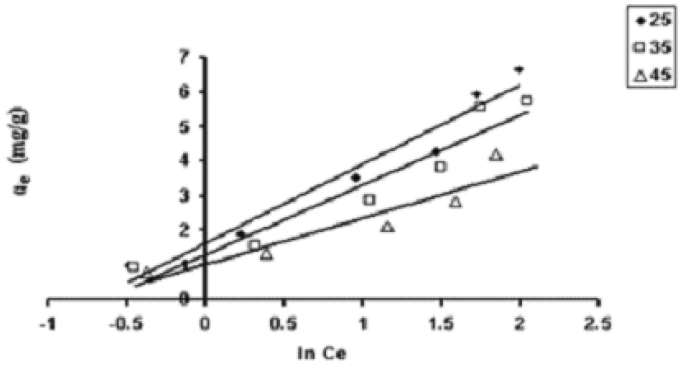

Fig. 9. Temkin isotherm for Cr(VI) uptake at three different temperatures.

Where R is the gas constant (JK^{-1} mol^{-1}), T is the temperature (K) and C_e is the equilibrium concentration (mg l^{-1}). When ln q_e values obtained at 25, 35 and 45°C, were plotted against ε^2, straight lines were obtained (Figure 8). The slopes of the linear plots yielded values of β which were used to calculate mean sorption energy E using the relationship

$$E = \frac{1}{\sqrt{-2B}}$$

which may be regarded as a free energy transfer of one mole of solute from infinity to the surface of an ILCMN sorbent. The numerical values of E, obtained at 25, 35 and 45°C, were found to be 8.97, 9.25 and 9.90 kJ mol^{-1}, respectively. As these values lie in the range of 8–16 kJ mol^{-1}, which is indicative of chemisorptions or an ion-exchange process, the Cr(VI) uptake on ILCMN sorbent may probably occur via the same mechanism. Finally, the uptake data was also fitted into the Temkin isotherm model which explicitly takes into account sorbate species-sorbent interactions. This isotherm assumes that: (i) the heat of sorption of all the molecules in the layer decreases linearly with coverage due to sorbate-sorbent interactions and (ii) adsorption is characterized by a uniform distribution of binding energies, up to some maximum binding energy. The Temkin equation is:

$$q_e = \beta_1 \ln K_t + \beta_1 \ln C_e$$

Where β_1 and K_t are the constants, K_t is the equilibrium binding constant (l mol^{-1}) corresponding to maximum binding energy and constant β_1 is related to sorption heat. Using the data obtained at three temperatures, q_e values may be plotted against ln C_e and straight lines are obtained (Figure 9). The slope and intercepts were used to calculate the constants $\beta_1$and K_t. All the isotherm constants, obtained for Freundlich, DKR and Temkin model have been given in the Table 2, along with corresponding regression values. It can clearly be seen that the Freundlich isotherm is most suitable to interpret the equilibrium sorption data.

3.6 Sorption Kinetics

In order to investigate the mechanistic aspects regarding the dynamics of the sorption process, chromium(VI) uptake was measured at different time-intervals for the ILCMN sorbent particles with size 84 and 508 μm at 25°C. The results as depicted in Figure 10, clearly indicate that the amount of Cr(VI) sorbed increases with time and later on, it attains an almost saturation value. The relatively higher uptake, observed for 84 μm sized particles as compared to 508 μm sized sorbent particles, may simply be attributed to the fact that smaller sized particles exhibit a greater surface area available and hence, provide more binding sites for uptake of Cr(VI) molecules. Here, it is worth mentioning that in our previous work (14), maximum Cr(VI) uptake, as exhibited by magnetite nanoparticles, was nearly 2.9 mg g^{-1}

Table 2. Data showing values of various constant obtained for different isotherm models using equilibrium sorption data obtained with 84 μm sized particles at different temperatures

	Freundlich constant			*Dubinin-Kaganer-Radudhkevich constant*			*Temkin constant*		
Temp. (°C)	K_F *(mg* g^{-1}*)* *(l* mg^{-1}*)*$^{1/n}$	*1/n*	R^2	$-\beta$	X_m	R^2	β_1	K_t	R^2
25	1.515	0.7683	0.9886	0.0062	1.13×10^{-6}	0.9922	2.2738	5.345	0.9513
35	1.266	0.7726	0.9907	0.0058	8.04×10^{-6}	0.9897	2.0365	4.3609	0.9243
45	1.006	0.7116	0.9869	0.0051	2.17×10^{-6}	0.982	1.3665	5.4053	0.8701

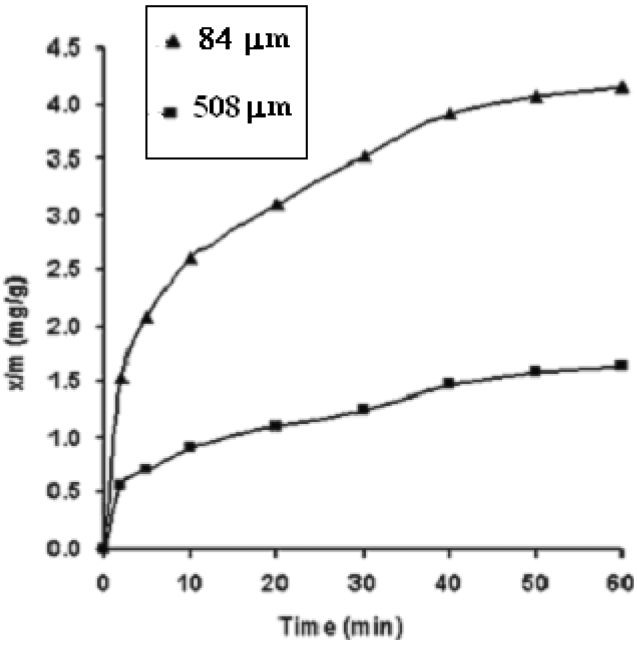

Fig. 10. The kinetic data for Cr(VI) uptake by sorbent particles of different size at 25°C.

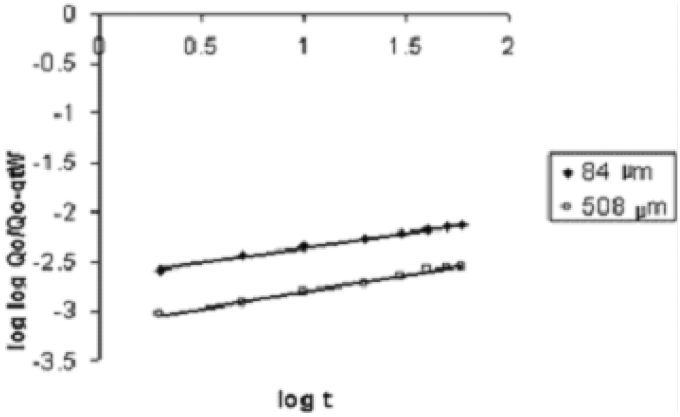

Fig. 12. Bangham equation showing intraparticle diffusion of Cr(VI) into sorbent particles of different sizes.

at 30°C, while in the present work, ILCMN sorbent particles with 84 μm diameter exhibit nearly 4.2 mg g^{-1} Cr(VI) uptake at 25°C. Therefore, this newly developed sorbent appears to be more effective than magnetite nanoparticles. A close look at Figure 10 also reveals that in the first 10 min, the sorption process is very rapid and nearly 60% of the total uptake is observed in this time span. However, after 10 min, the uptake process becomes relatively slower. The observed finding may be explained on the basis of the fact that initially Cr(VI) is sorbed simultaneously on the surface of the sorbent particles, thus making the uptake process fast. However, later on, the Cr(VI) molecules, which have been sorbed on the surface of the particles, begin to diffuse towards the bulk of the sorbent particles, thus causing intraparticle diffusion which occurs at a relatively slower rate. In order to further confirm this, graphs were plotted between log (time) and log (% sorption) which yielded fair linear plots (Figure 11), thus confirming the occurrence of intraparticle diffusion as suggested by Raghwanshi et al. (26). The higher regression values, i.e., 0.9961 and 0.9952 for 84 and 508 μm sized particles, also support excellent linearity observed. Thus, it can be concluded that 'intraparticle diffusion' does occur in the present study and it is the rate-limiting step (27). Finally, the intraparticle diffusion was also confirmed by applying dynamic uptake data on the Bangham equation (28) which is given as:

$$\log \log \, Q_0/Q_0 - q_t w = \log k_0 W/2.303\,V + a \log t$$

Where Q_0 is the initial concentration (g l^{-1}), of metal ion, V is the volume (l) of solution, W is the weight (g) of sorbent, q_t is the amount of Cr(VI) sorbed (g g^{-1}) at time, while α

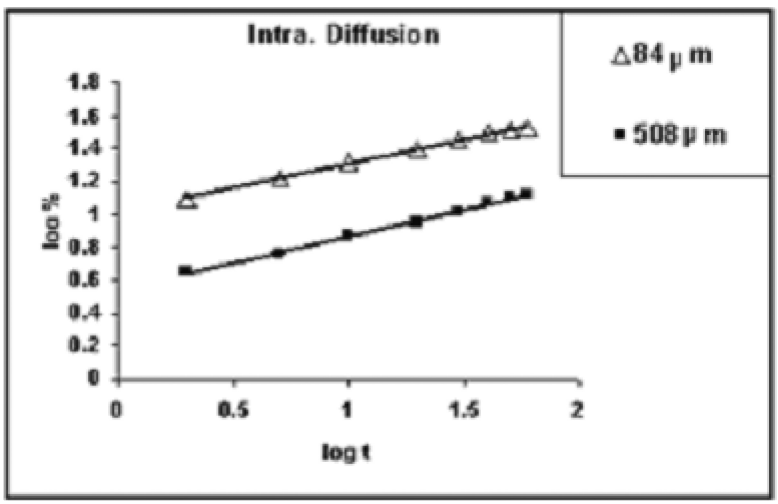

Fig. 11. Plot between log (% adsorption) and log (time) to confirm intraparticle diffusion of Cr(VI).

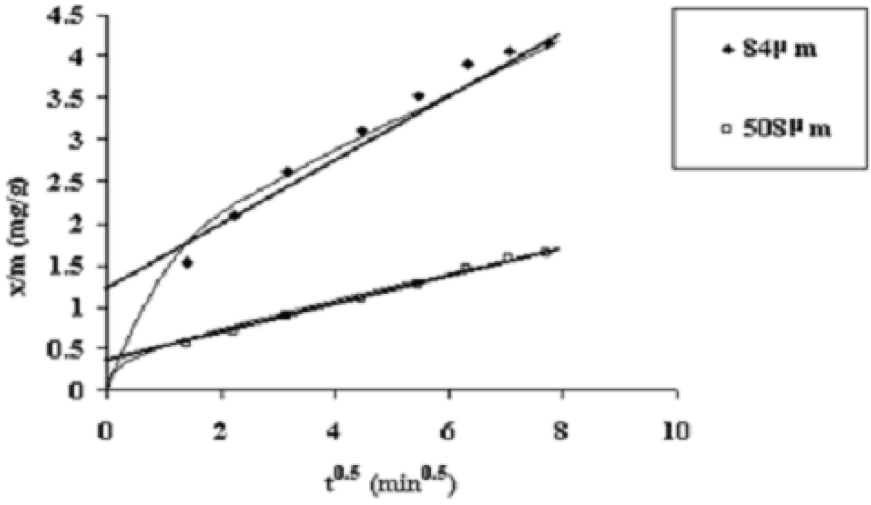

Fig. 13. q (mg g^{-1}) vs. $t^{0.5}$ plot for determination of k_{id} for Cr(VI) uptake by iron-loaded CMN particles of different sizes.

and k_0 are constant. Straight lines were obtained by plotting log log Q_0/Q_0-q_tw against log t (Figure 12) thus confirming the intraparticle diffusion of chromium (VI) into sorbent particles. We also calculated the rate constants for intraparticle diffusion, k_{id}, using the "intraparticle diffusion model" (29).

$$q = k_{id}\, t^{0.5} + I$$

Where q is amount of Cr(VI) sorbed (mg g^{-1}), at time t. The plots, obtained for Cr(VI) uptake by 84 and 508 μm sized sorbent particles at 25°C, are shown in Figure 13. The initial curved portion of the plots represents boundary layer adsorption, while the slope of the final linear portion is a measure of intraparticle diffusion. The regression values for the two plots, drawn for 84 and 508 μm sized particles, were found to be 0.9782 and 0.9959, respectively, thus indicating excellent fitness of the Weber-Morris equation on kinetic uptake data. The values of k_{id}at 25°C for 84 and 508 μm sized ILCMN particles were evaluated to be 41.56×10^{-2} and 17.48×10^{-2} mg g^{-1} $min^{-0.5}$, respectively. These values also establish superiority of this new sorbent over magnetite nanoparticles for which the k_{id} value was found to be in the range 9.6 to 20.0×10^{-2} mg g^{-1} $min^{1/2}$ in the temperature range of 30 to 50°C (14).

Finally, the kinetic uptake data at 25°C (as shown in Figure 10) was applied on various kinetic models, such as a first order kinetic model, second order uptake model, Lagergren equation, Power function model, Elovich equation (31) etc. Table 3 describes various constants obtained using these models along with their respective regression

Table 3. Data showing values of various constants obtained by applying different kinetic models on uptake of Cr(VI) by iron(III) loaded chitosan magnetite particles

			Parameters with	
S. No.	*Kinetic Model*	*Equation*	*84 μm*	*508 μm*
1	First Order	$-\ln (C/C_o) = kt$	$R^2 = 0.9409$ $K_1 = 0.0052$	$R^2 = 0.9720$ $K_1 = 0.0018$
2	Second Order	$1/C - 1/C_o$ kt	$R^2 = 0.9342$ $K_2 = 0.0012$	$R^2 = 0.9640$ $K_2 = .0004$
3	Lagergren Equation	$\ln (1 - q/q_e) = -k_{ad}.t$	$R^2 = 0.9666$ $k_{ad} = 0.0673$	$R^2 = 0.9358$ $k_{ad} = 0.0559$
4	Power Function	log q = log a + b log t	$R^2 = 0.9961$ a = 1.2817 b = 0.296	$R^2 = 0.9952$ a = 0.427 b = 0.3269
5	Simple Elovich	q = a + 2.303 b log t	$R^2 = 0.9893$ a = 0.8516 b = 0.8006	$R^2 = 0.9588$ a = 0.2172 b = 0.3286
6	Bangham Equation	log log $Q_o/Q_o - q_t$ W = log k_oW / 2.303V + α log t	$R^2 = 0.9959$ $\alpha = 0.3036$ $K_0 \times 10^3 = 12.6$	$R^2 = 0.9945$ $\alpha = 0.3353$ $K_0 \times 10^3 = 4.20$

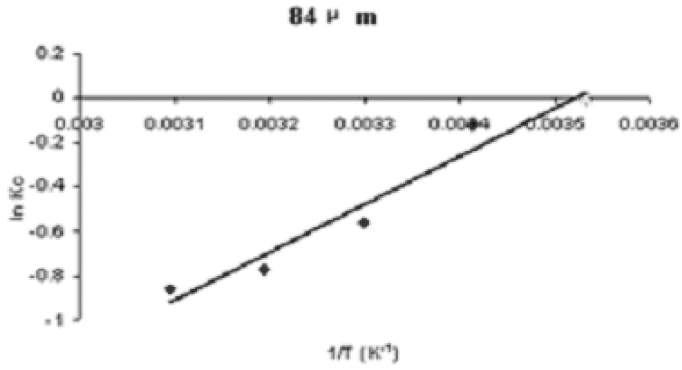

Fig. 14. In Kc vs. 1/T plot for evaluation of ΔH° and ΔS° for Cr(VI)uptake by sorbent particles with size 84 μm.

values. On the basis of regression values obtained for different models, it can be said that the Power function model appears to be the most suitable for the interpretation of uptake data. This, in turn, supports our findings that the equilibrium uptake of Cr(VI) is best interpreted by a Freundlich sorption isotherm because it has been supported that the Power function model, also known as modified the Freundlich equation (30), is a simple consequence of the Freundlich isotherm.

3.7 Evaluation of Thermodynamics Parameter

The various thermodynamic parameters were calculated for the sorption process using the following equations:

$$\Delta G^0 = -RT \ln K_c$$

Where K_c is the equilibrium constant for the sorption process and is given as:

$$K_c = C_0 - C_e/C_e$$

In addition, the values of ΔH^0 and ΔS^0 were calculated from the Van't Hoff equation given below:

$$\ln K_c = \Delta S/R - \Delta H/R.1/T$$

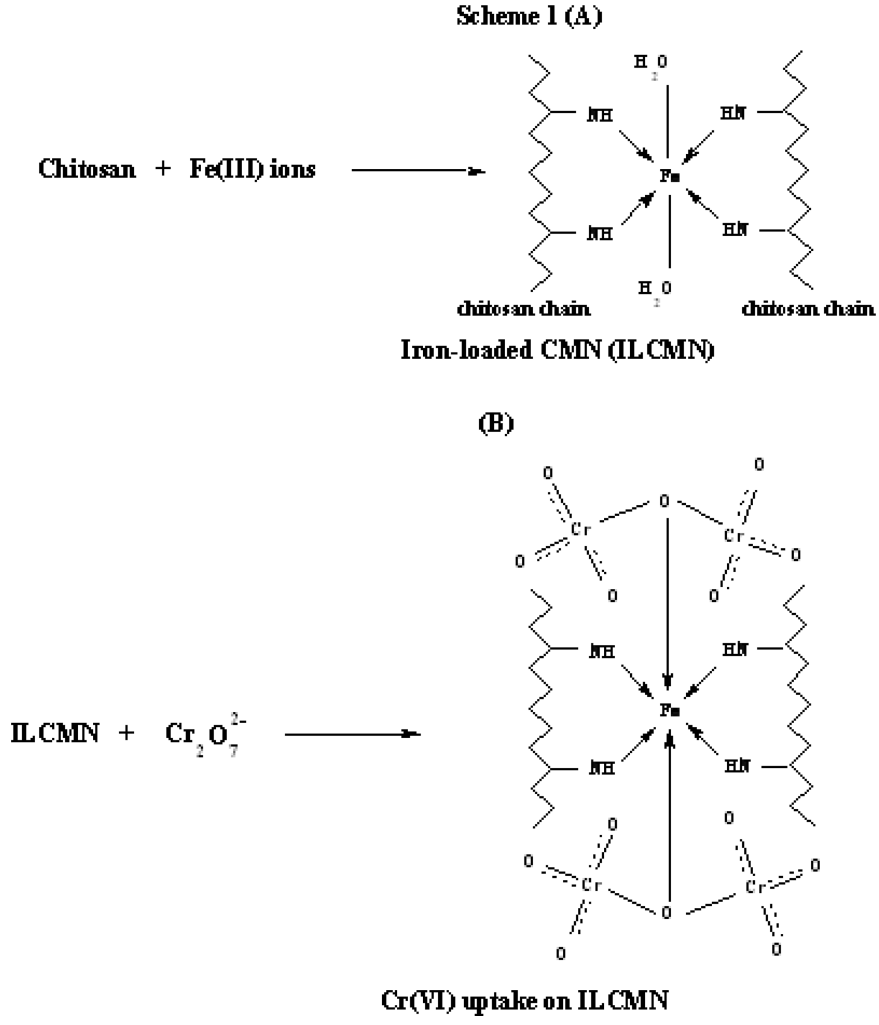

Sch 1. (A) Binding of Fe(III) ion with amino groups of two chitosan chains to form iron-loaded chitosan-magnetite nanocomposites (ILCMN). I (B) Coordination of $Cr_2O_7^{2-}$ ions with vacant sites present in (ILCMN).

By using the slope and intercept of linear plot obtained between ln K_c and 1/T for Cr(VI) uptake by 84 μm sized particles (Figure 14) the values of ΔH^0 and ΔS^0 were evaluated and found to be -0.063 kJ mol^{-1} and -17.87 kJ mol^{-1}, respectively. It is clear that negative ΔH^0 value is indicative of exothermic nature of the uptake process. In addition, negative value of ΔS^0 corresponds to the decrease in degree of freedom of the sorbed species (32). In other words, the coordinated water molecules, which are displaced by Cr(VI) ions, gain less translational entropy than is lost by Cr(VI) species, thus resulting in decreased randomness in the sorbent-sorbate interactions (33). The values of ΔS^0, obtained at 10, 20, 30, 40 and 50°C were 0.0162 0.309, 1.41, 2.01 and 2.30 kJ mol^{-1}, respectively.

3.8 Mechanism of Cr(VI) Uptake

Chromium exhibits different types of pH dependent equilibria in aqueous solutions e.g. below pH 1.0 it exists as H_2CrO_4, while in the pH range at 2 to 6, it has $HCrO_4^-$ and $Cr_2O_7^{2-}$as dominant species (34). In the present work, since the whole sorption studies have been carried out at self pH (i.e., pH 6.2) to make the overall process move practical and industrially feasible, the $Cr_2O_7^{2-}$ ions are the dominant species in the sorbate solution. It is well known that iron usually acts as trivalent cation Fe(III) to chelate with electronegative elements or electron donor species. Similar to Cu(II), iron(III) has also a stronger tendency to chelate with chitosan to form coordination compounds (34). With an electronic configuration of d^5, Fe(III) may form a more stable octahedral structure with six electron pair donors by the d^2sp^3 hybridization as reported elsewhere (35). On the basis of proposed coordination of Fe(III) with chitosan chains, the binding of chromium(VI) on this chitosan bound iron may be explained as shown in the Scheme 1. It is clear from Scheme 1 (A) that when Fe(III) ions come in contact with chitosan magnetite nanocomposite particles, iron (III) undergoes d^2sp^3hybridization to produce an octahedral structure and four nitrogen atoms of amino groups of two chitosan chains coordinate with iron(III) through coordination bonds. As can be seen, two coordination sites of Fe(III) are still vacant. Later on, when Fe(III) coordinated chitosan magnetite nanocomposite particles are agitated in Cr(VI) solution at self pH (i.e., 6.2), the 'O' atom present in $Cr_2O_7^{2-}$ ion, acting as bridge with two chromium atoms, coordinates with the vacant hybridized orbital of Fe(III). As there is an equal probability of coordination of $Cr_2O_7^{2-}$ with other vacant sites also, the overall chelating structure of Cr(VI) sorbed Fe(III)-chitosan complex may be shown as given in Scheme 1 (B). Therefore, the sorbtion of Cr(VI) onto Fe(III)-loaded chitosan magnetite nanocomposite particles appears to be chemical in nature.

4 Conclusions

From the above study, it may be concluded that after removal of iron(III) as a toxin from an aqueous solution by using chitosan-magnetite nanocomposites (CMN), the resulting iron(III)-loaded CMN obtained, may further be reused as a new sorbent material for magnetite separation of Cr(VI), the another potential toxin. This study opens the possibilities of using 'already used sorbent materials' for removal of metal ions.

References

1. Bajpai, S.K. (2001) *Sep. Sci. Technol.*, 36(3) 399.
2. Galvin, J.B. and Dberg, S.G. (1984) *Env. Res.*, 33, 7.
3. Bagchi, D., Stohs, S.J., Downs, B.W., Bagchi, M. and Preuss, H.G. (2003) *Toxiology*, 186(1–2), 171.
4. Baroni, P., Vieira, R.S., Meneghetti, F., de Silva M.G., and Beppa, M.M. (2008) *J. Hazard. Mater.*, 152(3), 1155.
5. Ansari, R. and Fahim, N.K. (2007) *React. Funct. Polym.*, 67, 367.
6. Abdel-Halim, E.S., Abou-Okeil A. and Hashem, A. (2006) *Polym. Plast. Technol. Eng.*, 4571.
7. Isa, M.H., Ibrahim, N., Aziz, H.A., Adlan, M.N., Sabiane, N.H., Zinatizadeh, A.A. and Kutty, S.R. (2008) *J. Hazard. Mater.*, 152(2), 662.
8. Namasivayam, C. and Sureshkumar, M.V. (2008) *Bio. Resour. Technol.*, 99(7), 2218.
9. Arslan, G. and Pehliuan, E. (2007) *Bioresour. Technol.*, 98(15), 2836.
10. Fiol, N., Poch J., and Villaescusa, I. (2004) *Chem. Sep. Bioavail.*, 16(1/2), 25.
11. Ahalya, N., Kanamadi R.D. and Ramachandra, T.V. (2007) *J. Environ. Biol.*, 28(4), 765.
12. Krishnani, K.K., Parimala, V., and Meng, X. (2004) *Water SA.*, 30(4), 541.
13. Yean, S. and Cong, L. (2005*) J. Mater. Res.*, 20(12), 3255.
14. Bajpai, S.K. and Namdeo, M. (2008) *EJEFchem.*, 7(7), 3082.
15. Hu, J., Chem., G. and Lo, I.M.C. (2005) *Water Res.*, 39(18), 4528.
16. Ngomsik, A., Bee, A., Siaugue, J., Cabuit, V. and Cote, G. (2006) *Water Res.*, 40, 1848.
17. Sheha, R.R. and El- Zahhar, A.A. (2008) *J. Hazardous Mater.*, 150(3), 795.
18. Bajpai, S.K. and Namdeo, M. (2008) *Colloids and Surfaces A. Physicochem. Eng. Aspects*, 320, 161.
19. Bajpai, S.K. and Tankhiwale, R. (2006) *J. Macromol. Sci., Part A, Pure and Appl. Chem.*, 43, 1.
20. Bajpai, S.K. and Namdeo, M. (2007) *J. of Bionano.*, 1, 131.
21. APHA. Standard methods for Examination of water and waste water 17th Ed., American Public Health Association: New York (1989).
22. Findon, A., Mckay, G. and Blair, H.S. (1993) *J. Environ. Sci. Health: A*, 28(1), 173.
23. Badmus, M.A.O., Audu, T.O.K. and Anyator, B.U. Turkish (2001) *J. Eng. Env. Sci.*, 31, 251.
24. Singh, R., Shah, A.V. and Shah, B. (2007) *Sorption E-J-Chem.*, 4(4), 587.
25. Ahmad, S., Khalid, N. and Daud, M. (2002) *Sep. Sci. Technol.*, 37(2), 343.
26. Raghuwanshi, S.P., Singh, R. and Kaushik, C.P. (2004) *Appl. Ecolo. Environmental Res.*, 2(2), 35.
27. Knocke, W.R. and Hemphill, L.H. (1981) *Water Res.*, 15, 275.
28. Rehman, H., Shakirullah, M., Ahmad, I., Shah, S. and Hameedullah, J. (2006) *Chinese Chem. Soc.*, 53, 1045.

29. El-Ashtoukhy, E.S.Z., Amin, N.K. and Abdelwahab, O. (2008*) Desalination*, 223, 162.
30. Wahba, M.M. and Zaghloul, A.M. (2007) *J. Appl. Sci. Res.*, 3(6), 421.
31. Singh, T.S., Parikh, B. and Pant, K.K. (2006) *Water SA*, 32(1), 49.
32. Unnithan, M.R., Vinod, V.P. and Anirudhan, T.S. (2002) *J. Appl. Polym. Sci.*, 84, 2541.
33. Alaya, N., Kanamadi, R.D. and Ramchandran, T.V. (2005) *Electronic J. Biotechnol*, 8(3), 257.
34. Burke, A., Yilmaz, E. and Hasirci, N. (2000) *Tur. J. Chem.*, 30341.
35. Bhatia, S.C. and Ravi, N. (2000) *Biomacromolecules*, 1(3), 413.